Electron relay via diffusible and protein-bound flavin cofactor in human six-transmembrane epithelial antigen of the prostate (STEAP)

Kehan Chen[1,*], Lie Wang[1,*], Jiemin Shen[1], Ah-lim Tsai[2], Ming Zhou[1,#], Gang Wu[2,#]

[1] Verna and Marrs McLean Department of Biochemistry and Molecular Biology, Baylor College of Medicine, Houston, Texas 77030, United States

[2] Division of Hematology-Oncology, Department of Internal Medicine, University of Texas-McGovern Medical School, Houston, Texas 77030, United States

* These authors contributed equally

[#] Corresponding authors: gang.wu@uth.tmc.edu and mzhou@bcm.edu

Author Contribution Statement

GW and MZ initiated and designed the project. KC and LW led the effort of protein production and structure determination and with help from JS and GW. GW designed and conducted spectroscopic measurements. All authors analyzed and interpreted the data. GW and MZ wrote the manuscript with inputs from all authors.

Data and Materials availability

The EM data and fitted model of human STEAP2 have been deposited in the Electron Microscopy Data Bank (EMD-25775) and the RCSB Protein Data Bank (7TAI).

Abstract

Six transmembrane epithelial antigen of the prostate (STEAP) is a family of membrane-embedded metal ion reductases that transfer electrons across the cell membranes. STEAPs are unique to mammals and implicated in metabolic and inflammatory responses and are significantly upregulated in many types of cancer cells. There are four members in the family, STEAP1 – 4, and all STEAPs have a transmembrane domain (TMD) that has a conserved heme binding site, and STEAP2 – 4, but not STEAP1, have an intracellular reductase domain (RED) that binds to NADPH and FAD. NADPH, FAD, and heme form an electron transfer chain that allows electron flow across the cell membranes, however, the mechanism of the stepwise cross-membrane electron transfer remains unclear. It is also unclear how STEAP1, which does not have a RED, acquires and transfers electrons. We expressed and purified human STEAP2 (hSTEAP2), and constructed the electron transfer chain *in vitro*. Purified hSTEAP2 mediates electron transfer from NADPH to FAD and to heme, with a NADPH oxidation rate of 2.6×10^{-3} s^{-1}. The time course for reduction of heme is more complex with an initial rate of ~ 1.6×10^{-4} s^{-1}. We also found that the heme in hSTEAP2 has a low-spin electron structure and thus a rigid coordination, which is consistent with its high occupancy in the purified protein and its role as part of the electron transfer chain. We then determined the structure of hSTEAP2 in complex with $NADP^+$, FAD, and heme by cryo-electron microscopy to 3.2 Å. Human STEAP2 forms a homotrimer and its structure is similar to that of hSTEAP4. $NADP^+$, FAD, and heme are well-resolved in the structure, and while the current conformation would allow electron transfer from FAD to heme, the FAD isoalloxazine ring is ~ 19 Å away from NADPH and does not support hydride transfer. Significant structural changes are required to accommodate dissociation of the FAD isoalloxazine ring from the TMD such that the FAD may become diffusible after its

reduction. To test this hypothesis and also to find out how STEAP1 may transfer electrons, we reconstructed an electron transfer chain for STEAP1 and found that the heme in STEAP1 can be reduced by FAD produced either by the full-length STEAP2 or by the soluble RED domain from STEAP4. These results support a “diffusible FAD” mechanism and demonstrate that STEAP1 is capable of mediating electron transfer across the cell membranes. In summary, our study established a structural and functional framework for further analyses for resolving the mechanism of electron transfer in STEAPs.

Introduction

Six transmembrane epithelial antigen of the prostate (STEAP) proteins, which contain four members, STEAP1 – 4, are membrane-embedded hemoproteins that transfer electrons across the cell membranes to reduce ferric and cupric ions, functioning as metalloreductases.[1, 2] STEAPs are implicated in the endosomal transferrin cycle in erythroid cells, controlling the trafficking and availability of iron and copper, [3, 4] and are significantly upregulated in many types of cancer cells.[5-7] STEAP family of proteins belong to a large superfamily of membrane-embedded reductases which include mammalian NADPH oxidases (NOX) and dual oxidases (DUOX), and bacterial and yeast ferric reductases (FRE).[8] This superfamily of proteins all have a transmembrane domain (TMD) with six transmembrane helices. The TMD in NOX, DUOX, and FRE binds two heme prosthetic groups, each ligated to a pair of conserved histidine residues in the TMD; one heme is close to the intracellular side and another close to the extracellular side of the membrane. In contrast, STEAP proteins have only a single pair of conserved histidine residues which ligate to one heme near the extracellular side of the membrane. Binding of a single heme was previously shown by spectroscopic analysis of rabbit STEAP1 (rSTEAP1) [9] and human STEAP3 (hSTEAP3)[10] , and more recently by the cryo-electron microscopy (cryo-EM) structures of human STEAP1 (hSTEAP1) [11] and human STEAP4 (hSTEAP4).[12] The structure of hSTEAP4 confirms that the single heme is close to the extracellular side, and in addition, shows that the isoalloxazine ring of FAD occupies a position similar to the heme close to the intracellular side of the TMD in NOX and DUOX.[12-14]

NOX, DUOX, and FRE all have an intracellular soluble reductase domain (RED) that binds both NADPH and FAD and catalyzes NADPH to FAD hydride transfer. Similarly, STEAP2 – 4 have a N-terminal RED, which is much smaller than the REDs found in NOX or DUOX, while

STEAP1 does not have a RED. Crystal structures of the isolated REDs from hSTEAP3 and rat STEAP4 show only a binding site for NADPH,[15, 16] and the structure of the full-length hSTEAP4 confirms the NADP(H) binding site on the RED and shows that the FAD is coordinated mainly by residues from the TMD and only has a tenuous interaction with the RED through a stacking interaction between its adenosine moiety and a tryptophan from the RED. [12]

The dimeric structures of DUOX show that the FAD isoalloxazine ring aligns with the NADPH nicotinamide ring to acquire electrons and then donates the electrons to the heme near the intracellular side of the TMD in the same protomer; continuous flow of electrons from NADPH to FAD to hemes may be achieved with little or no structural changes.[13, 14] In STEAP proteins, the flow of electrons likely is discontinuous because the FAD has to "shuttle" between alternative conformations to be near either the NADPH or the heme.[12] Individual electron transfer reaction has not been measured in STEAPs, nor has other mechanisms been explored. In addition, STEAP1, which was first identified because of its abnormally high expression level on prostate cancer cells and is the namesake of this family of proteins, mysteriously lacks a RED.[5] In a previous study, we showed that STEAP1 can form heterotrimers with STEAP2 and thus may sustain electron transfer by appropriating electrons from the RED of STEAP2. However, other mechanisms by which STEAP1 may acquire electrons have not been explored.

In this study, we expressed and purified full-length human STEAP2 (hSTEAP2). We reconstructed a fully functional electron transfer chain *in vitro* and demonstrated the reduction of heme in hSTEAP2 using NADPH. We determined the structure of hSTEAP2 by cryo-EM. We also demonstrated that the heme in STEAP1 can receive electrons from diffusible $FADH_2$ from either STEAP2 homotrimer or from isolated RED of STEAP4. Based on these results, we proposed that STEAP proteins transfer electrons in two non-mutually exclusive pathways.

Materials and Methods

Materials 4-(2-hydroxyethyl)-1-piperazineethanesulfonic acid (HEPES), 5-aminolevulinic acid (5-ALA), isopropyl β-D-1-thiogalactopyranoside (IPTG), phenylmethanesulfonyl fluoride (PMSF), $FeCl_3$, hemin chloride, dithionite, and ferricyanide were from Sigma-Aldrich (St. Louis, MO). Lauryl maltose neopentyl glycol (LMNG) and glyco-diosgenin (GDN) were from Anatrace (Maumee, OH).

Cloning, expression, and purification of STEAPs. The hSTEAP2 gene (NCBI accession number AAN04080.1) was codon optimized and cloned into a modified pFastBac Dual expression vector for production of baculovirus according to the Bac-to-Bac method (Thermo Fisher Scientific, Waltham, MA). P3 viruses were used to infect High Five (*Trichoplusia ni*) or sf9 (*Spodoptera frugiperda*) insect cells at a density of ~ 3×10^6 cells mL^{-1} in the media including 0.5 mM 5-ALA, 10 μM $FeCl_3$, and 5 μM hemin chloride. Infected cells were grown at 27 ºC for 48 – 60 h before harvest. Cell membranes were prepared using a hypotonic/hypertonic wash protocol as previously described.[17] Purified cell membrane pellets were then flash-frozen in liquid nitrogen for further use.

Purified membranes were thawed and homogenized in 20 mM HEPES, pH 7.5 buffer containing 150 mM NaCl, and then solubilized with 1.5% (w/v) LMNG at 4 ºC for 2 h. After solubilization, cell debris was removed by ultracentrifugation (55,000 × g for 45 min at 4 ºC), and hSTEAP2 was purified from the supernatant using cobalt-based Talon affinity resin (Clontech, Mountain View, CA). The C-terminal His_6-tag was cleaved with tobacco etch virus (TEV) protease at room temperature for 30 min. The protein was concentrated to around 5 mg mL^{-1} using an Amicon spin concentrator with a 100 kDa cut-off (Millipore, Burlington, MA), and then loaded onto a SRT-3C SEC-300 size-exclusion column (Sepax Technologies, Newark,

DE) equilibrated with 20 mM HEPES buffer containing150 mM NaCl and 0.01% (w/v) LMNG. For the sample used in the cryo-EM structural studies, the size-exclusion column was equilibrated with 20 mM HEPES buffer containing 150 mM NaCl and 0.02% GDN.

Rabbit STEAP1 (NCBI accession number NP_001164745.1) was expressed and purified following the methods published previously.[9]

Expression and purification of hSTEAP4 RED. The construct of the cytosolic RED of hSTEAP4, residues 1 – 203, was cloned into a modified pET vector with an N-terminal His_{10}-tag and a TEV protease cleavage site. The vector was the transformed into *Escherichia coli* BL21(DE3) cells, and the transformed cells were grown in Luria–Bertani (LB) medium at 37 ºC till the optical density at 600 nm reached 0.8 – 1. Protein overexpression was induced by adding 0.5 mM IPTG, followed by shaking at 20 ºC for 16 hr. The cells were harvested by centrifugation and resuspended in 20 mM HEPES pH 7.5 containing 150 mM NaCl and 1 mM PMSF.

To purify the hSTEAP4 RED, the resuspended cells were lysed by sonication, and the lysate was cleared by ultracentrifugation at 55,000 x g for 45 min at 4 ºC. The protein was then purified from the supernatant using cobalt-based Talon affinity resin. The His-tag was cleaved with TEV protease at room temperature for 30 min. The protein was then concentrated to around 5 mg mL^{-1} using Amicon spin concentrator with a 10 kDa cut-off, and loaded onto the SRT-3C SEC-300 size-exclusion column equilibrated with 20 mM HEPES pH 7.5 and 150 mM NaCl.

Electronic absorption and magnetic circular dichroism (MCD) spectroscopy of hSTEAP2. UV-Vis spectra of hSTEAP2 were recorded using a Hewlett-Packard 8452 or a 8453 diode-array spectrophotometer (Palo Alto, CA). The extinction coefficient of the heme was determined by pyridine hemochrome assay as published previously.[9] MCD spectra of hSTEAP2 were recorded

with a Jasco J-815 CD spectropolarimeter (Tokyo, Japan). The magnetic field was provided with an Olis permanent magnet (Bogart, GA) and the field strength was calibrated with a ferricyanide solution using A_{420} = 3.0 $M^{-1}cm^{-1}T^{-1}$. MCD measurements were conducted at room temperature with the parameters: spectral bandwidth, 5 nm; time constant, 0.5 s; data pitch, 0.5 nm; scan speed, 200 nm/min. Each MCD spectrum is an average of 12 repetitive scans. MCD intensity was expressed as molar difference absorption coefficient, ΔA, in units of $M^{-1}cm^{-1}$ $tesla^{-1}$.

Cryo-EM sample preparation and data collection of hSTEAP2. Quantifoil R1.2/1.3 Cu grids were glow-discharged in air for 15 s at 10 mA in a plasma cleaner (PELCO EasiGlow, Ted Pella, Inc., Redding, CA). Glow-discharged grids were prepared using Thermo Fisher Vitrobot Mark IV. Concentrated hSTEAP2 (3.5 μl) was applied to each glow-discharged grid. After blotted with filter paper (Ted Pella, Inc.) for 4.0 s, the grids were plunged into liquid ethane cooled with liquid nitrogen. A total of 7509 micrograph stacks were collected using SerialEM[18] on a Titan Krios electron microscope (Thermo Fisher) at 300 kV with a Quantum energy filter (Gatan, Pleasanton, CA), at a nominal magnification of 105,000× and with defocus values of −2.5 μm to −0.8 μm. A K3 Summit direct electron detector (Gatan) was paired with the microscope. Each stack was collected in the super-resolution mode with an exposing time of 0.175 s per frame for a total of 50 frames. The dose was about 50 e^- per $Å^2$ for each stack. The stacks were motion-corrected with MotionCor2[19] and binned (2 × 2) so that the pixel size was 1.08 Å. Dose weighting[20] was performed during motion correction, and the defocus values were estimated with Gctf.[21]

Cryo-EM data processing. A total of 4,210,570 particles were automatically picked (RELION 3.1)[22-24] from the motion-corrected images and imported into cryoSPARC.[25] After 2 rounds of two-dimensional (2D) classification, a total of 91 classes containing 1,031,895 particles were

selected. A subset of 12 classes containing 117,053 particles were selected for *ab initio* three-dimensional (3D) reconstruction, producing one good class with recognizable structural features and three bad classes with no distinct structural features. Both the good and bad classes were used as references in the heterogeneous refinement (cryoSPARC) and yielded a good class at 4.10 Å from 305,849 particles. Non-uniform refinement (cryoSPARC) was then performed with C3 symmetry and an adaptive solvent mask, producing a map with an overall resolution of 3.16 Å. Resolutions were estimated using the gold-standard Fourier shell correlation with a 0.143 cut-off[26] and high-resolution noise substitution.[27] Local resolution was estimated using ResMap.[28]

Model building and refinement of hSTEAP2 structure. The structural model of hSTEAP2 was built based on the cryo-EM structure of hSTEAP4 (PDB ID: 6HCY),[12] and the side chains were adjusted based on the density map. Model building was conducted in Coot.[29] Structural refinements were carried out in PHENIX in real space with secondary structure and geometry restraints.[30] The EMRinger Score was calculated as described.[31]

Reduction of the heme by NADPH. Human STEAP2, 2.3 μM, or a mixture of 1.1 μM hSTEAP2 and 0.9 μM rSTEAP1 (all the concentrations were based on ferric heme absorbance) was pre-incubated with 2.5 and 2.2 μM FAD, respectively, and placed in a tonometer. The solutions were made anaerobic by 5 anaerobic cycles, each with 30 s vacuum followed by 4.5 min argon displacement. The stock solution of NADPH was made anaerobic by passing N_2 though the solution. Anaerobic NADPH solution was then added to the anaerobic STEAP solution using an airtight syringe and the spectral changes were monitored at 25 ^{o}C using the Hewlett-Packard 8453 spectrophotometer. The same procedure was followed to determine the electron transfer from hSTEAP4 RED to rSTEAP1; 1.5 μM rSTEAP1 was mixed with 1.5 μM hSTEAP4 RED, and 2.2 μM FAD and the mixed proteins were reacted with 55 μM NADPH anaerobically.

Results

Expression and purification of hSTEAP2. The purified hSTEAP2 showed a single band on SDS-PAGE (Fig. S1). The size-exclusion chromatography of hSTEAP2 exhibited a peak consistent with molecular weight between ~100 – 150 kD (Fig. S1), indicating that hSTEAP2 forms a homotrimer, which was later confirmed by the structure of hSTEAP2. The heme content in purified hSTEAP2 typically ranged from 70 – 90%. FAD was also detected in the purified hSTEAP2, however, its level showed stronger batch-dependence varying from 0.3 – 19 %, determined based on the fluorescence of FAD released from denatured purified hSTEAP2 (data not shown). No NADP(H) was detected in the purified hSTEAP2, suggesting that its association with hSTEAP2 is more transient than FAD or heme.

Characterization of the heme in hSTEAP2. The ferric heme in hSTEAP2 showed a Soret band at 413 nm and unresolved α/β bands centered around 550 nm (Fig. 1A). Upon dithionite reduction, the Soret band shifted to 427 nm and the α and β bands split to be well resolved at 560 and 532 nm, respectively (Fig. 1A). These UV-Vis spectral features are consistent with a bis-imidazole ligated *b*-type cytochrome.

We further characterized the heme using magnetic circular dichroism (MCD) spectroscopy. The MCD spectrum of ferric hSTEAP2 was consistent with a low-spin heme with strong Soret signals between 404 nm to 419 nm and a crossover at 412 nm, a trough at 575 nm and no high-spin charge-transfer signal at wavelength above 600 nm (Fig. 1B). The MCD spectrum of ferrous hSTEAP2 exhibited a very strong α band from 554 nm to 562 nm with the crossover at 557 nm, and a minor α/β band between 512 nm and 535 nm with a crossover at 531

nm (Fig. 1B), consistent with the intense A-term Faraday effect of typical low-spin *b* type heme. On the other hand, the Soret band MCD of ferrous hSTEAP2 was significantly weaker than that of ferric hSTEAP2 (Fig. 1B). Overall, both UV-Vis and MCD data indicated that the heme is in the low-spin state in both oxidized and reduced hSTEAP2, the same as in STEAP1[9] and in STEAP3 and STEAP4 (unpublished data). The rigid low-spin heme in STEAPs is in consistent with its role in electron transfer.

Cryo-EM structure of hSTEAP2. We determined the structure of hSTEAP2 in the presence of $NADP^+$ and FAD by cryo-EM to an overall resolution of 3.2 Å. The density map was of sufficient quality to allow *de novo* building of all the major structural elements of hSTEAP2 (Fig. S2&3). The final model consists of residues 28 – 331 and 350 – 469 (Fig. 2). The N-terminal residues 1 – 27, C-terminal residues 470 – 490, and residues 331 – 350 are not resolved in our EM map, likely due to their flexibility. The unresolved N- and C-terminal residues are in the regions that show low similarity among STEAP2, 3, and 4. In the structures of STEAP4 and STEAP1, the residues corresponding to hSTEAP2 residues 331 – 350 (residues 319 – 338 in hSTEAP4 and residues 190 – 209 in hSTEAP1) form a short extracellular helix followed by a loop which connects transmembrane helices TM3 and TM4.[11, 12]

Human STEAP2 forms a homotrimer with each protomer consisted of an N-terminal cytosolic RED connected to the TMD through a short loop (Fig. 2). As in hSTEAP4, hSTEAP2 homotrimer shows a domain-swapped quaternary structure, where the RED of one protomer extends underneath the TMD of a neighboring protomer (Fig. 2 a & b). RED in STEAP2 – 4 share sequence homology to archaeal $F_{420}H_2$:$NADP^+$ oxidoreductase (FNO).[12, 15, 16] The TMD in hSTEAP2 consists of six transmembrane helices, TM1 – 6, with three extracellular loops and two intracellular loops (Fig. 2). Overall, the TMD of hSTEAP2 has an RMSD (Cα) of 0.8 Å to

hSTEAP4 and its TMD has an RMSD (Cα) of 0.98 Å to hSTEAP1. [11, 12]

In the density map of hSTEAP2, heme, FAD, and $NADP^+$ can be clearly identified (Figs. 2c and S2). We also found densities that likely correspond to bound lipid molecules. An ordered phospholipid molecule was built between the TMDs of two neighboring protomers, and cholesterol molecules were built on the periphery of each TMD (Fig. S2). These tightly bound lipid molecules likely have structural roles such as supporting the trimerization and stability of the structural fold, and may regulate functions of STEAP.

$NADP^+$ in hSTEAP2. The $NADP^+$ molecule is contained within the RED of hSTEAP2 in an extended conformation through several polar and hydrophobic interactions (Fig. 3). The adenine ring of $NADP^+$ stacks with His97 while the guanidinium group of Arg61 forms hydrogen bond with the phosphate on the 2'-OH of the adenosine moiety. The mainchain NH of His42 and Asp40 interact with the 3'-OH of the adenosine and pyrophosphate group of $NADP^+$, respectively. The 2'- and 3'-OH groups of the ribose connected to the nicotinamide ring interact with the mainchain NH and C=O of Asn118 and Ile93, respectively. The nicotinamide ring of $NADP^+$ is held in place through the interactions of its amide group with mainchain C=O of Ser150 and stacked with Phe41. Overall, the nicotinamide ring of $NADP^+$ is close to the TMD but remains ~9 Å and 18.6 Å away from the FAD adenine and isoalloxazine rings in the neighboring protomer, respectively (Fig. 2e).

Heme in hSTEAP2. The heme in hSTEAP2 binds in a pocket facing the extracellular side of the membrane (Fig. 4). The iron atom in heme is ligated to the sidechains of two strictly conserved histidine residues, His316 in TM3 and His409 in TM5 (Fig. 4A), with the two histidine imidazole rings roughly parallel each other. As in hSTEAP1 and hSTEAP4, the vinyl groups of the porphyrin ring face towards the center of TMD in hSTEAP2, having hydrophobic

interactions with serval residues, while the two propionate groups of the porphyrin ring extend towards the extracellular side (Fig. 4A). The propionate from the C-ring has polar interactions with Lys257-$N^{\zeta}H_3^+$ while the propionate from the D-ring interacts with Asn256-$CONH_2$.

Right above the heme propionates on the extracellular side, several positively charged sidechains, including those of Arg233, Lys249, Lys257, Arg326, Arg356, and Arg417, formed a positively-charged ring (Fig. 4B). These charges are conserved in hSTEAP4 and have been proposed to form the binding site for negatively charged complex ions of ferric or cupric ions to facilitate metal ion reduction.[12]

Conformation of the FAD in hSTEAP2. The FAD molecule adopts an extended conformation and straddles both TMD and RED (Fig. 5), similar to that in the structure of hSTEAP4.[12] The adenosine moiety of FAD is located at the interface between the TMD and the RED of a neighboring protomer, while the isoalloxazine ring protrudes deep inside the TMD towards the heme. Although the bulk of the FAD molecule is buried inside the TMD, its adenine ring stacks on Trp152 from the RED (Fig. 5A). The adenosine 2'-OH group is within hydrogen bond distance to Lys462-$N^{\zeta}H_3^+$ from the TMD, which helps to hold the adenosine in position (Fig. 5A). The interactions with the FAD pyrophosphate come from the sidechains of Arg302, Ser392, Ser396, Tyr400, and Lys446 from the TMD (Fig. 5A). The ribitol of FAD could form hydrogen bond to the phenol hydroxyl from Tyr291. Deep inside the TMD, the FAD isoalloxazine ring interacts extensively with hSTEAP2 residues (Fig. 5B). Other than the hydrophobic interactions of isoalloxazine C^7-CH_3 and C^8-CH_3 groups with Leu307 and Leu374, strong polar interactions include N^5 with Ser378-OH and Gln395-$CONH_2$, C^4=O with Ser378-OH, N^{10} with Gln395-$CONH_2$, and the interactions between N^3H and C^2=O with Asp160-COO^- from the RED of the neighboring protomer (Fig. 5B).

The C^8-CH_3 of FAD is ~10 Å away from the vinyl group on the B-ring of the heme (Fig. 2e). The sidechain of Leu371 protrudes approximately midway between the FAD isoalloxazine ring and the heme (Fig. 4A). This leucine is conserved in both hSTEAP1 (Leu230) and hSTEAP3 (Leu371) but substituted by a phenylalanine in hSTEAP4 (Phe359). In hSTEAP4, Phe359 ring has been proposed to mediate electron transfer from $FADH_2$ to the heme;[12] We speculate that Leu371 plays a similar role in mediating electron transfer from FAD to heme. On the other hand, the extended conformation of the FAD positions its isoalloxazine ring 18.6 Å away from the nearest nicotinamide ring of the $NADP^+$, too far to accept hydride from the nicotinamide ring of NADPH.

Heme reduction in hSTEAP2 by NADPH. We implemented an assay to monitor the reduction of heme by NADPH in hSTEAP2. We first pre-incubated hSTEAP2 with FAD under anaerobic conditions and then reacted it with NADPH; the reaction was conducted in the absence of O_2 to avoid the re-oxidation of $FADH_2$ by O_2. During the reaction, the Soret absorbance shifted from wavelength of ferric heme (413 nm) to that of ferrous heme (427 nm), and the α and β became well resolved at 560 nm and 532 nm, respectively, indicating the reduction of the bound heme (Fig. 6). In the meantime, the oxidation of NADPH was clearly shown by the concomitant decrease in its absorbance (A_{340}) (Fig. 6). The spectral change of FAD was not clearly resolved due to the large heme background at the FAD absorbance wavelength (450 nm). The oxidation of NADPH, which reflects the convolution of both hydride transfer to FAD and reduction of heme, was a single-exponential process with a rate of 2.6×10^{-3} s^{-1} (Fig. 6, inset). On the other hand, the time courses of spectral changes of both A_{413} and A_{427}, which reflects the reduction of heme, were more complicated and could not be fit with exponential function. We estimated that the initial (200 s) decay of A_{413} has a rate of ~ 1.6×10^{-4} s^{-1}. The complex time courses of heme

Soret absorbance were likely due to other reaction step(s) unresolved from the heme reduction kinetics (Fig. 6, inset).

Electron transfer from STEAP RED to the heme in STEAP1. We were curious if the $FADH_2$ produced in STEAP2 could reach STEAP1, which does not have its own RED, and reduces the heme in STEAP1. We mixed hSTEAP2 with about equal amount of rSTEAP1 and pre-incubated the proteins with FAD. We then made the mixture anaerobic and reacted it with NADPH (60 μM) anaerobically. As in the reaction of hSTEAP2 with NADPH, the Soret absorbance shifted from that of ferric heme to ferrous heme (Fig. 7). At the end of the reaction, a narrow Soret absorbance at 427 nm was observed with no shoulder at 413 nm (Fig. 7), indicating that all the heme, in both hSTEAP2 and rSTEAP1, was completely reduced. The concomitant oxidation of NADPH was also observed based on the decrease of A_{340} (Fig. 7). This result indicated that hSTEAP2 can supply electrons to the heme in rSTEAP1. As in the case of hSTEAP2 (Fig. 6, inset), the time course of NADPH oxidation follows a simple exponential process, with a rate of 7.7×10^{-4} s^{-1} (Fig. 6, inset). The decay initial (300 s) of A_{413} was estimated to be ~ 1.7×10^{-4} s^{-1}. On the other hand, the time courses of both A_{413} and A_{427} are more complicated and could not be fit with simple exponential functions (Fig. 7, inset).

We then examined whether STEAP1 can receive electrons from the isolated RED of a STEAP protein. We used hSTEAP4 RED for this experiment since chimeric $STEAP1_{TMD}$-$STEAP4_{RED}$ protein has been shown to have metalloreductase activity.[12] We mixed rSTEAP1, isolated hSTEAP4 RED, and FAD and reacted the mixture with NADPH under anerobic condition, and found that the Soret peak of rSTEAP1 shifted from 413 nm to 426 nm and A_{340} of NADPH decreased in the reaction, indicating the reduction of the heme in rSTEAP1 by NADPH (Fig. S4). The oxidation of NADPH by the isolated hSTEAP4 RED had a much slower rate of

2.6×10^{-4} s^{-1} (Fig. S4, inset), and the initial rate (300 s) of heme reduction was also significantly slower at ~ 8.1×10^{-5} s^{-1}.

Discussion

In this study, we determined the structure of hSTEAP2, demonstrated that the bound heme has a rigid low-spin electron structure, and implemented an assay to monitor electron transfer from NADPH via FAD to heme (Fig. 6). Although metal ion reduction has been demonstrated in STEAP family of proteins,[2] direct observation for the change in redox state of the two cofactors and heme have not been previously reported. Our study paved the way for a more precise dissection of each electron transfer step and thus a better understanding of the mechanism in STEAPs.

The orientation of the heme porphyrin ring in hSTEAP2 and the proximity of the FAD isoalloxazine ring provide a structural basis for analysis of electron transfer from FAD to heme. The FAD isoalloxazine ring is ~ 10 Å away from the heme, a distance too large for direct electron transfer; the electron transfer is likely mediated by Leu371, which is found about halfway between the FAD and heme (Fig. 4). Since the equivalent residue in hSTEAP4 is a phenylalanine, further studies are required to resolve how leucine or phenylalanine may relay the electrons.

The structure of hSTEAP2 shows that the isoalloxazine ring of FAD is ~18.6 Å away from the nicotinamide ring of NADPH in the neighboring RED and ~32.3 Å away from the nicotinamide in the same subunit (Fig. 2e). Similar distances were also observed in the structure of hSTEAP4. Such large distances do not support direct hydride transfer from NADPH to FAD. The FAD likely adopts a different conformation with its isoalloxazine ring stacked with the

nicotinamide ring for hydride transfer. Gros *et al* has proposed a "FAD-shuttling" mechanism in which the FAD switches between the extended conformation observed in the hSTEAP4 structure and a folded conformation with the isoalloxazine ring coming out of its binding pocket in the TMD to stack on the nicotinamide ring in RED; electrons are shuttled from NADPH to the heme through this FAD conformational switch (Scheme 1, A and B).[12] A hypothetic channel for the FAD isoalloxazine ring to move into and out of the hSTEAP4 TMD was also proposed.[12] We agree with this hypothesis in principle, however, we propose that structural change in STEAP is required, especially at the interface between the TMD and RED to accommodate the movement of the isoalloxazine ring (Scheme 1, B). Opening up of the interface between TMD and RED may also allow diffusion and therefore direct access of reduced $FADH_2$, and we show that this mechanism could work in STEAP1, which does not have a RED (Scheme 1, B and C). Since the FAD isoalloxazine ring is stabilized in the TMD by the interactions with several residues, the factor(s) governing the FAD conformational switch remains unresolved. We hypothesize that the structural changes required for FAD conformational switch could be driven by the binding of NADPH or redox changes of the cofactors or the heme, or a combination of both. Further structural and functional studies are required to resolve the mechanism.

Both STEAP1 and STEAP2 are expressed at high level in prostate cancer cells.[1, 7] We previously showed that STEAP1 and STEAP2 can form heterotrimers when co-expressed.[9] In heterotrimers of STEAP1 and STEAP2, electrons from the NADPH bound to the RED of STEAP2 could conceivably reach the heme in the TMD of STEAP1 because of the domain-swapped assembly of STEAP trimers, and thus enabling transmembrane flow of electron through STEAP1. The structures of hSTEAP2 and hSTEAP4 led us to realize that the RED domain may partially dissociate from the TMD to allow entry and exit of FAD to the TMD, and led us to

propose a “diffusible FAD” mechanism (Scheme 1, B and C). The reduction of heme in STEAP1 in its mixture with either STEAP2 homotrimers or isolated STEAP4 RED indicate that reduced $FADH_2$ can dissociate from a STEAP RED and that STEAP1 can utilize the $FADH_2$ in solution to reduce its heme (Figs. 7 and S4). Thus the formation of heterotrimers of STEAP1 with other STEAPs such as STEAP2 is not a prerequisite for STEAP1 to obtain electrons in cells. Although the “diffusible FAD” mechanism (Scheme 1, B and C) is supported by these initial tests, more precise *in vitro* measurements and cell-based assays are needed to provide more a conclusive verdict. Our discovery of inter-STEAP electron transfer has strong implications for the function of STEAP1, which mysteriously lacks a RED, and for the mechanism of electron transfer in STEAP2 – 4 that possess a functional RED.

Reference

[1] Grunewald, T. G., Bach, H., Cossarizza, A., and Matsumoto, I. (2012) The STEAP protein family: versatile oxidoreductases and targets for cancer immunotherapy with overlapping and distinct cellular functions, *Biol Cell 104*, 641-657.

[2] Ohgami, R. S., Campagna, D. R., McDonald, A., and Fleming, M. D. (2006) The Steap proteins are metalloreductases, *Blood 108*, 1388-1394.

[3] Knutson, M. D. (2007) Steap proteins: implications for iron and copper metabolism, *Nutr Rev 65*, 335-340.

[4] Ji, C., and Kosman, D. J. (2015) Molecular mechanisms of non-transferrin-bound and transferring-bound iron uptake in primary hippocampal neurons, *J Neurochem 133*, 668-683.

[5] Hubert, R. S., Vivanco, I., Chen, E., Rastegar, S., Leong, K., Mitchell, S. C., Madraswala, R., Zhou, Y., Kuo, J., Raitano, A. B., Jakobovits, A., Saffran, D. C., and Afar, D. E. (1999) STEAP: a prostate-specific cell-surface antigen highly expressed in human prostate tumors, *Proc Natl Acad Sci U S A 96*, 14523-14528.

[6] Gomes, I. M., Santos, C. R., Socorro, S., and Maia, C. J. (2013) Six transmembrane epithelial antigen of the prostate 1 is down-regulated by sex hormones in prostate cells, *Prostate 73*, 605-613.

[7] Rocha, S. M., Barroca-Ferreira, J., Passarinha, L. A., Socorro, S., and Maia, C. J. (2021) *The Usefulness of STEAP Proteins in Prostate Cancer Clinical Practice*, Exon Publications, Brisbane, Australia.

[8] Zhang, X., Krause, K. H., Xenarios, I., Soldati, T., and Boeckmann, B. (2013) Evolution of the ferric reductase domain (FRD) superfamily: modularity, functional diversification, and signature motifs, *PLoS One 8*, e58126.

[9] Kim, K., Mitra, S., Wu, G., Berka, V., Song, J., Yu, Y., Poget, S., Wang, D. N., Tsai, A. L., and Zhou, M. (2016) Six-Transmembrane Epithelial Antigen of Prostate 1 (STEAP1) Has a Single b Heme and Is Capable of Reducing Metal Ion Complexes and Oxygen, *Biochemistry 55*, 6673-6684.

[10] Kleven, M. D., Dlakic, M., and Lawrence, C. M. (2015) Characterization of a single b-type heme, FAD, and metal binding sites in the transmembrane domain of six-transmembrane epithelial antigen of the prostate (STEAP) family proteins, *J Biol Chem 290*, 22558-22569.

[11] Oosterheert, W., and Gros, P. (2020) Cryo-electron microscopy structure and potential enzymatic function of human six-transmembrane epithelial antigen of the prostate 1 (STEAP1), *J Biol Chem 295*, 9502-9512.

[12] Oosterheert, W., van Bezouwen, L. S., Rodenburg, R. N. P., Granneman, J., Forster, F., Mattevi, A., and Gros, P. (2018) Cryo-EM structures of human STEAP4 reveal mechanism of iron(III) reduction, *Nat Commun 9*, 4337.

[13] Sun, J. (2020) Structures of mouse DUOX1-DUOXA1 provide mechanistic insights into enzyme activation and regulation, *Nat Struct Mol Biol 27*, 1086-1093.

[14] Wu, J. X., Liu, R., Song, K., and Chen, L. (2021) Structures of human dual oxidase 1 complex in low-calcium and high-calcium states, *Nat Commun 12*, 155.

[15] Sendamarai, A. K., Ohgami, R. S., Fleming, M. D., and Lawrence, C. M. (2008) Structure of the membrane proximal oxidoreductase domain of human Steap3, the dominant

ferrireductase of the erythroid transferrin cycle, *Proc Natl Acad Sci U S A 105*, 7410-7415.

[16] Gauss, G. H., Kleven, M. D., Sendamarai, A. K., Fleming, M. D., and Lawrence, C. M. (2013) The crystal structure of six-transmembrane epithelial antigen of the prostate 4 (Steap4), a ferri/cuprireductase, suggests a novel interdomain flavin-binding site, *J Biol Chem 288*, 20668-20682.

[17] Bai, Y., McCoy, J. G., Levin, E. J., Sobrado, P., Rajashankar, K. R., Fox, B. G., and Zhou, M. (2015) X-ray structure of a mammalian stearoyl-CoA desaturase, *Nature 524*, 252-256.

[18] Mastronarde, D. N. (2005) Automated electron microscope tomography using robust prediction of specimen movements, *J Struct Biol 152*, 36-51.

[19] Zheng, S. Q., Palovcak, E., Armache, J. P., Verba, K. A., Cheng, Y., and Agard, D. A. (2017) MotionCor2: anisotropic correction of beam-induced motion for improved cryo-electron microscopy, *Nat Methods 14*, 331-332.

[20] Grant, T., and Grigorieff, N. (2015) Measuring the optimal exposure for single particle cryo-EM using a 2.6 A reconstruction of rotavirus VP6, *Elife 4*, e06980.

[21] Zhang, K. (2016) Gctf: Real-time CTF determination and correction, *J Struct Biol 193*, 1-12.

[22] Kimanius, D., Forsberg, B. O., Scheres, S. H., and Lindahl, E. (2016) Accelerated cryo-EM structure determination with parallelisation using GPUs in RELION-2, *Elife 5*.

[23] Scheres, S. H. (2012) RELION: implementation of a Bayesian approach to cryo-EM structure determination, *J Struct Biol 180*, 519-530.

[24] Scheres, S. H. (2015) Semi-automated selection of cryo-EM particles in RELION-1.3, *J Struct Biol 189*, 114-122.

[25] Punjani, A., Rubinstein, J. L., Fleet, D. J., and Brubaker, M. A. (2017) cryoSPARC: algorithms for rapid unsupervised cryo-EM structure determination, *Nat Methods 14*, 290-296.

[26] Rosenthal, P. B., and Henderson, R. (2003) Optimal determination of particle orientation, absolute hand, and contrast loss in single-particle electron cryomicroscopy, *J Mol Biol 333*, 721-745.

[27] Chen, S., McMullan, G., Faruqi, A. R., Murshudov, G. N., Short, J. M., Scheres, S. H., and Henderson, R. (2013) High-resolution noise substitution to measure overfitting and validate resolution in 3D structure determination by single particle electron cryomicroscopy, *Ultramicroscopy 135*, 24-35.

[28] Kucukelbir, A., Sigworth, F. J., and Tagare, H. D. (2014) Quantifying the local resolution of cryo-EM density maps, *Nat Methods 11*, 63-65.

[29] Emsley, P., Lohkamp, B., Scott, W. G., and Cowtan, K. (2010) Features and development of Coot, *Acta Crystallogr D Biol Crystallogr 66*, 486-501.

[30] Adams, P. D., Afonine, P. V., Bunkoczi, G., Chen, V. B., Davis, I. W., Echols, N., Headd, J. J., Hung, L. W., Kapral, G. J., Grosse-Kunstleve, R. W., McCoy, A. J., Moriarty, N. W., Oeffner, R., Read, R. J., Richardson, D. C., Richardson, J. S., Terwilliger, T. C., and Zwart, P. H. (2010) PHENIX: a comprehensive Python-based system for macromolecular structure solution, *Acta Crystallogr D Biol Crystallogr 66*, 213-221.

[31] Barad, B. A., Echols, N., Wang, R. Y., Cheng, Y., DiMaio, F., Adams, P. D., and Fraser, J. S. (2015) EMRinger: side chain-directed model and map validation for 3D cryo-electron microscopy, *Nat Methods 12*, 943-946.

Scheme and Figure Legends

Scheme 1. **Hypothetic electron pathways in STEAPs.** (A) In the structures of hSTEAP2 and hSTEAP4 homotrimers, the FAD in the extended conformation straddles the TMD of a protomer (grey shaded) and the RED of a neighboring protomer (pink shaded). The adenine ring of FAD stacks with Trp152 in the RED and the isoalloxazine ring protrudes into the TMD. The heme binds in the TMD and NADP(H) binds in the RED. (B) The FAD adopts a hypothetic folded conformation with the isoalloxazine ring stacked with the nicotinamide ring of NADPH for hydride transfer. The hypothetic "FAD-shuttling" mechanism[12] is based on the movement of the FAD isoalloxazine ring between the TMD and the RED. Significant structural changes may be required to accommodate the conformational switch of the FAD and such structural changes may allow the dissociation and rebinding of FAD(H_2). Purple arrows represent the conformational switch of the FAD. (C) The $FADH_2$ generated in the REDs of STEAP2 – 4 homotrimers or in an isolated RED may dissociate and diffuse to the TMD of STEAP1; STEAP1-bound $FADH_2$ can transfer electrons to the heme. Blue arrows represent the dissociation and binding of $FADH_2$. Yellow, heme; orange, FAD; green, NADP(H); olive, Trp152.

Figure 1. **UV-Vis and MCD spectra of hSTEAP2.** The UV-Vis (A) and MCD (B) spectra of hSTEAP2 are plotted with absorbance in $mM^{-1}cm^{-1}$ and MCD in $M^{-1}cm^{-1}Tesla^{-1}$, respectively. Black, ferric hSTEAP2 and red, ferrous hSTEAP2.

Figure 2. **Cryo-EM structure of hSTEAP2.** The sharpened density map (a) and cartoon presentation (b) for hSTEAP2 homotrimer. Top, the side view of hSTEAP2 homotrimer, and the color bar represents the membrane; "in", intracellular side and "out', extracellular side. Bottom, the top view of hSTEAP2 homotrimer from the extracellular side. (c) The structure of one hSTEAP2 protomer. Left, side view and right, top view from the extracellular side. (d) The

topographic representation of the secondary structural elements. Bar, helix and arrow, β strand. Dashed lines represent the unresolved segments. (e) Schematic representation of the spatial relationship of $NADP^+$, FAD, and heme. Grey shade, TMD and pink shade, RED.

Figure 3. **The $NADP^+$ in hSTEAP2 RED.** The $NADP^+$ molecule is represented by sticks. The sidechains of several interacting residues are also plotted, His97 stacked with the $NADP^+$ adenine ring, Arg61 hydrogen-bound to 2'-phosophate on the adenosine moiety, and Phe41 stacked with the nicotinamide ring.

Figure 4. **The heme in hSTEAP2.** (A) The heme is ligated to His316 and His409, on TM3 and TM5, respectively. Leu371, which is found in the midway between the heme and the FAD isoalloxazine ring, is also plotted. (B) The arginine and lysine residues which form the hypothetic binding site for the ferric or cupric complex ion substrates.

Figure 5. **Binding of the FAD in hSTEAP2.** (A) Several residues that interact with the adenosine moiety and pyrophosphate of FAD are plotted. Lys462 that interacts with 2'-OH of the adenosine and Arg302 and Tyr400 with the pyrophosphate are from the TMD (cyan) while Trp152 stacking with the adenine ring is from the RED of a neighboring protomer (wheat). (B) The residues that interact significantly with the FAD isoalloxazine ring are plotted. Gln395 that interacts with N^5 and N^{10}, Ser378 that interacts with N^5 and O^4, and Leu374 that has hydrophobic interactions with the methyl groups are from the TMD (cyan) and Asp160 that interacts with N^5 and O^2 is from the RED of the neighboring protomer (wheat).

Figure 6. **UV-Vis spectral change during the reaction of hSTEAP2 with NADPH.** Human STEAP2, 2.3 μM, was pre-incubated with 2.5 μM FAD and then reacted anaerobically with 45 μM NADPH at 25 °C. The direction of spectral change is indicated by the arrows. Blue, the spectrum captured right after hSTEAP2(FAD) was mixed with NADPH; red, the last spectrum of

the kinetic measurement. Inset, the time courses of A_{340} (NADPH, circle), A_{413} (ferric heme, triangle), and A_{427} (ferrous heme, square). Red, monophasic fit of the time course of A_{340}.

Figure 7. **UV-Vis spectral change during the reaction of the mixture of rSTEAP1 and hSTEAP2 with NADPH.** The mixture of 1.1 μM hSTEAP2 and 0.9 μM rSTEAP1 was pre-incubated with 2.2 μM FAD and then reacted anaerobically with 60 μM NADPH at 25 °C. The direction of spectral change is indicated by the arrows. Blue, the spectrum captured right after the mixture of hSTEAP2 and rSTEAP1(FAD) was reacted with NADPH; red, the last spectrum of the kinetic measurement. Inset, the time courses of A_{340} (NADPH, circle), A_{413} (ferric heme, triangle), and A_{427} (ferrous heme, square). Red, monophasic fit of the time course of A_{340}.

Scheme 1

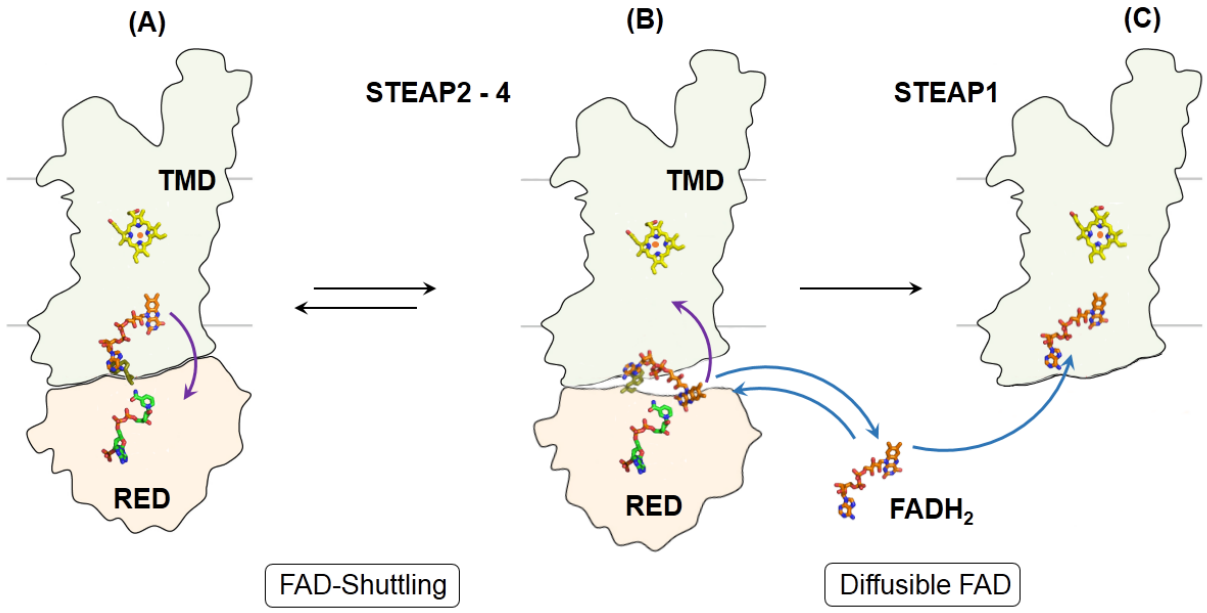
(A)
(B)
(C)
STEAP2 - 4
STEAP1
TMD
TMD
RED
RED
FADH2
FAD-Shuttling
Diffusible FAD

Figure 1

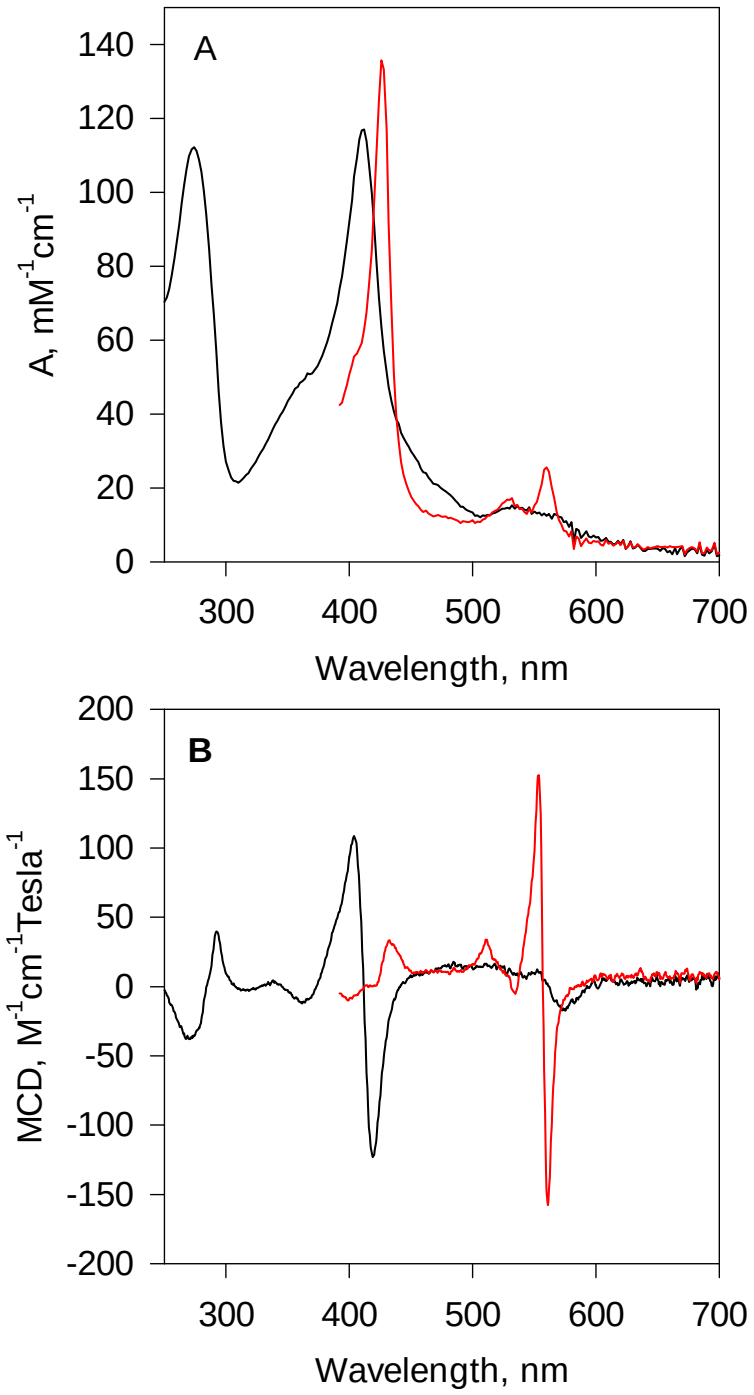
A
140
120
100
80
60
40
20
0
A, mM-1cm-1
300
400
500
600
700
Wavelength, nm
B
200
150
100
50
0
-50
-100
-150
-200
MCD, M-1cm-1Tesla-1
300
400
500
600
700
Wavelength, nm

Figure 2

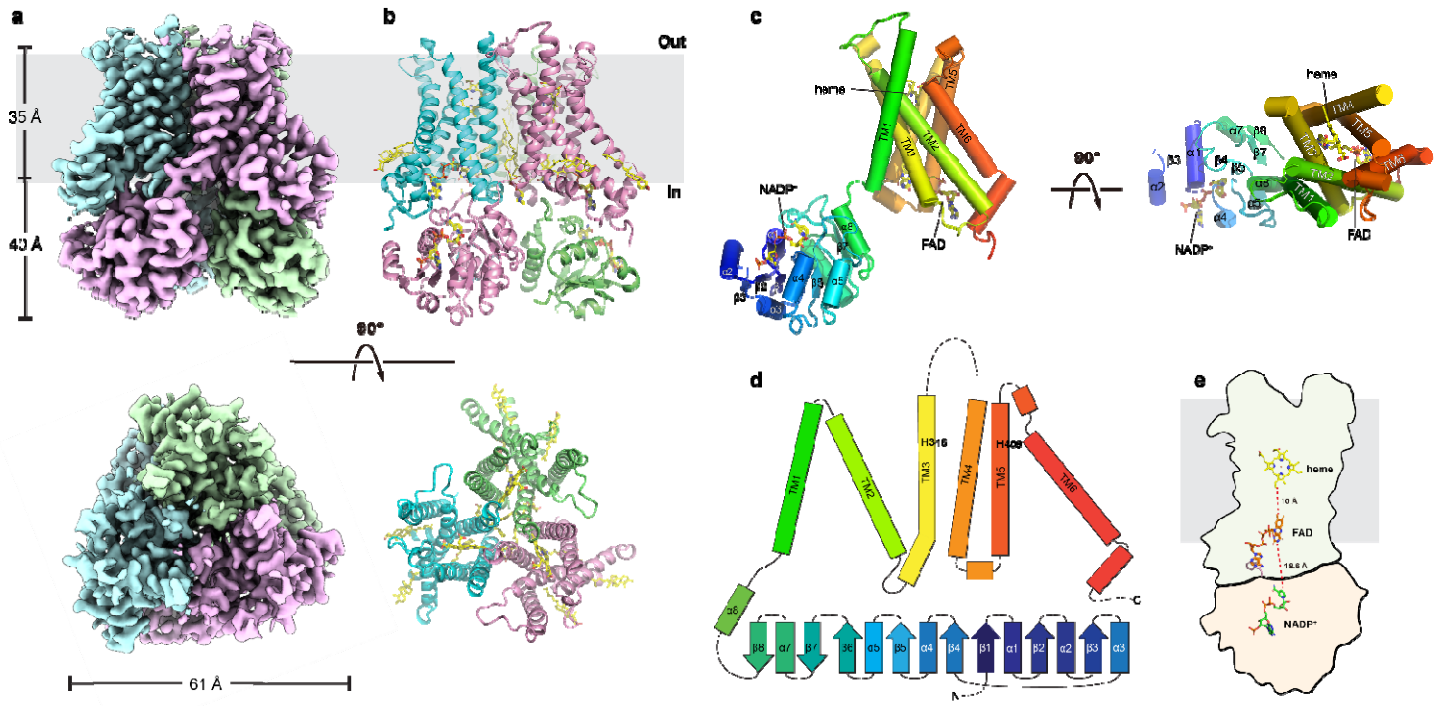

a
b
c
d
e
35 Å
40 Å
Out
In
90°
61 Å
heme
NADP+
FAD
TM1
TM2
TM3
TM4
TM5
TM6
H316
H409

Figure 3

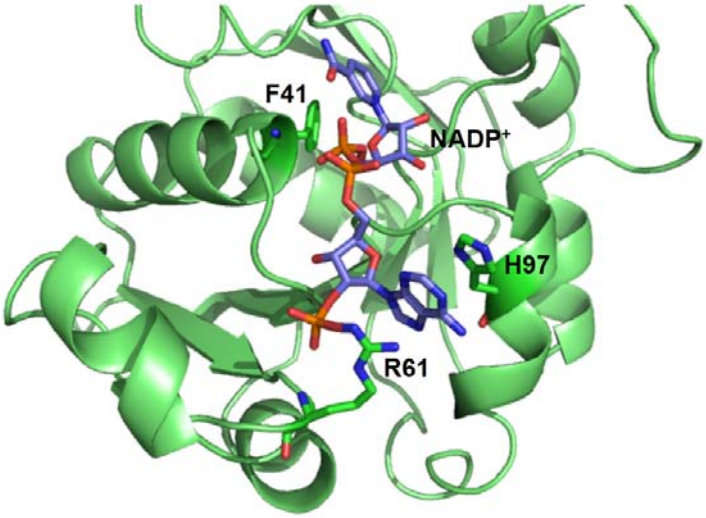

Figure 4

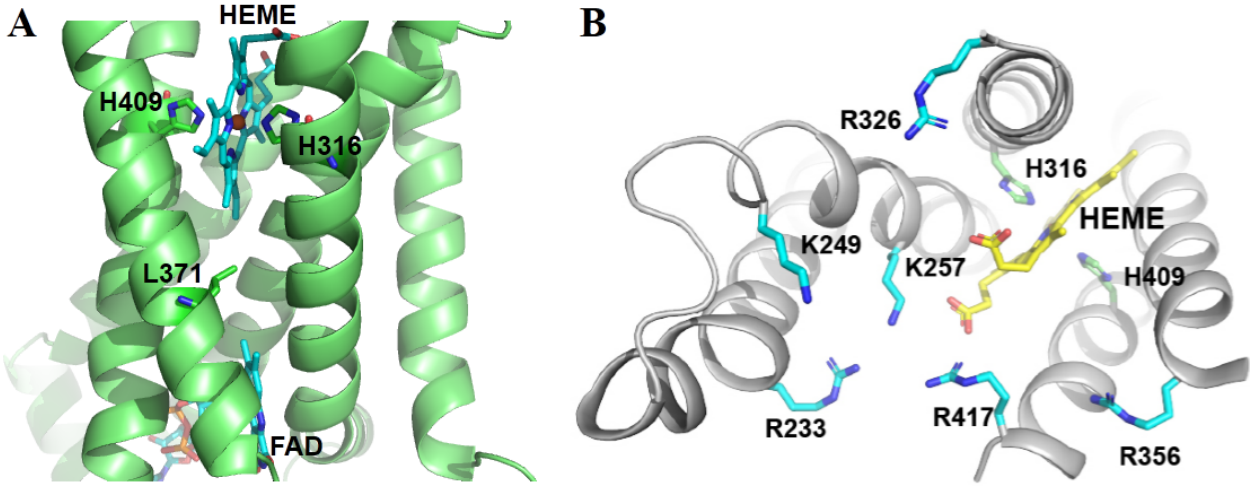
A
HEME
H409
H316
L371
FAD
B
R326
H316
HEME
K249
K257
H409
R233
R417
R356

Figure 5

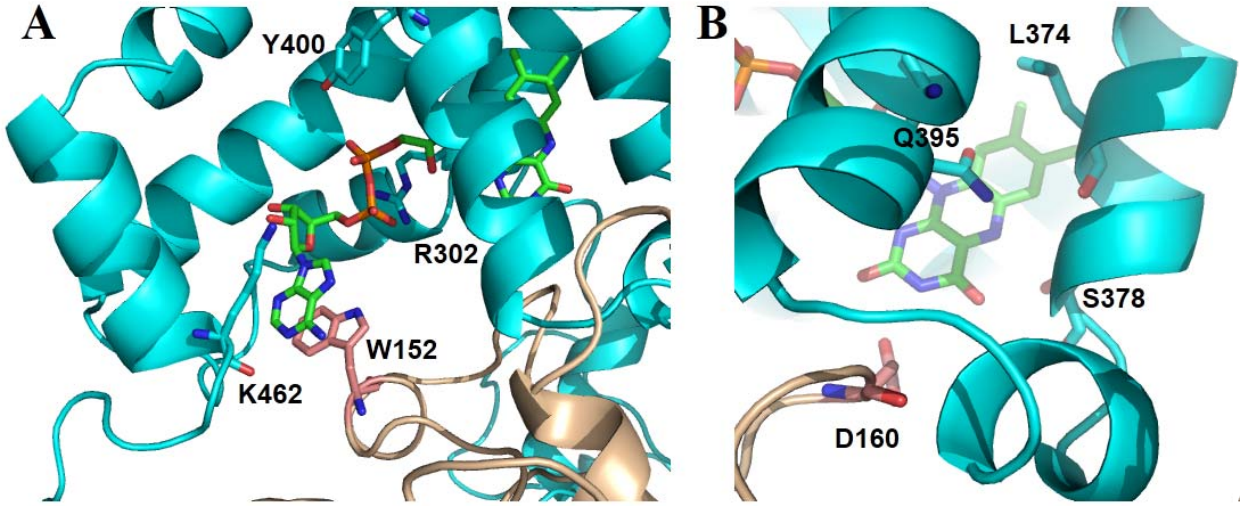

Figure 6

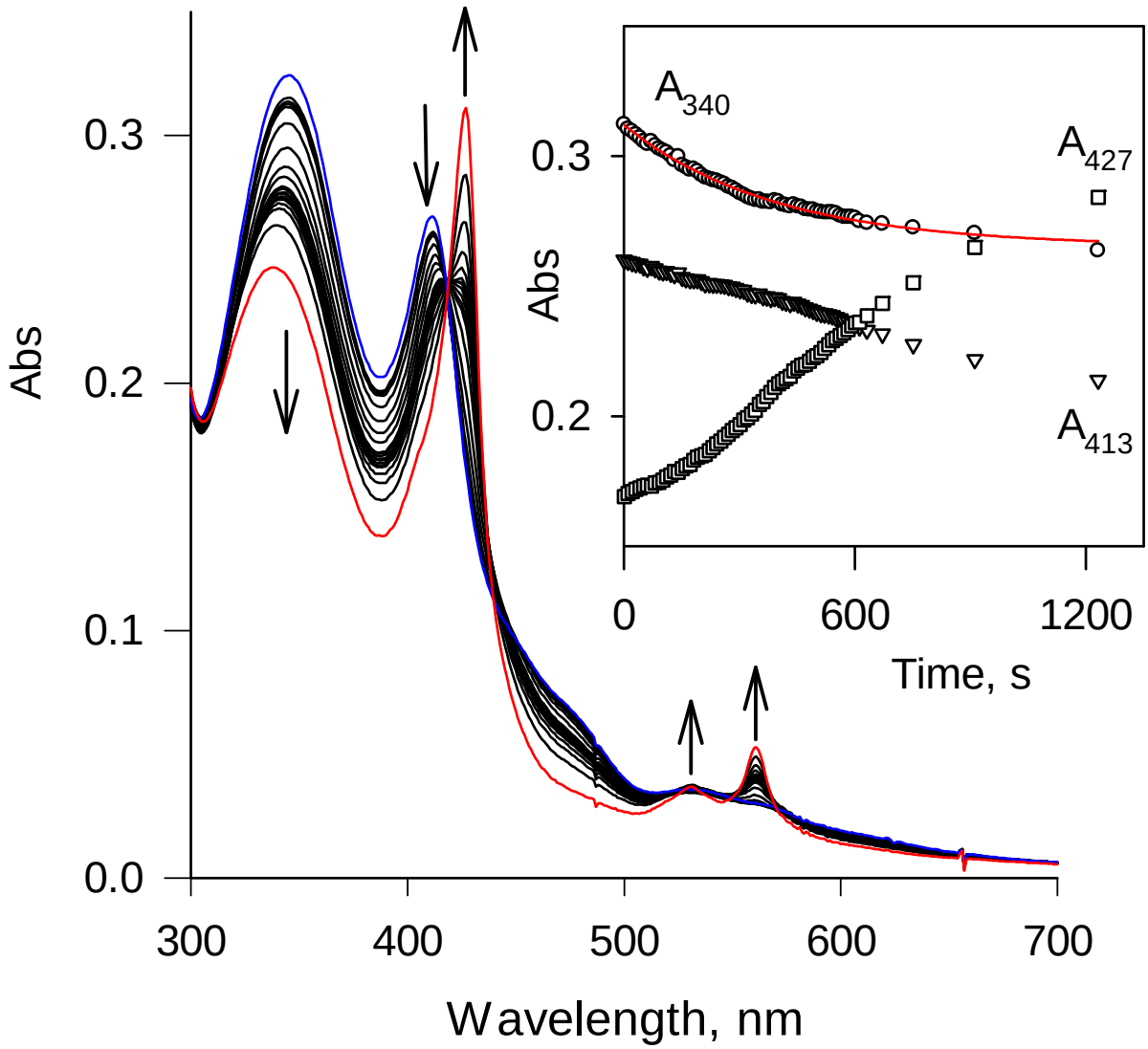
Abs
0.0
0.1
0.2
0.3
300
400
500
600
700
Wavelength, nm
A340
A427
A413
Abs
0.2
0.3
0
600
1200
Time, s

Figure 7

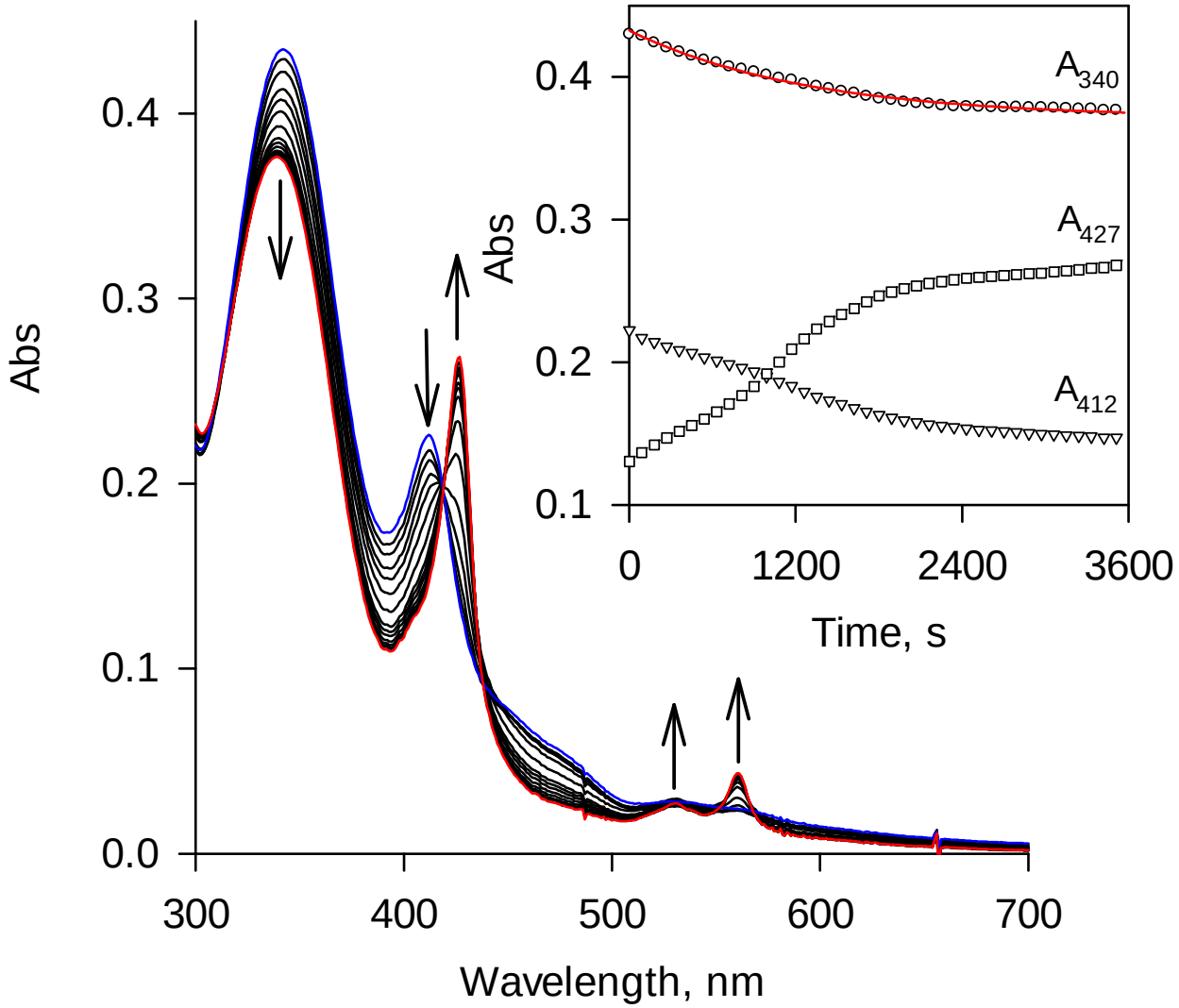
Abs
0.0
0.1
0.2
0.3
0.4
300
400
500
600
700
Wavelength, nm
Abs
0.1
0.2
0.3
0.4
0
1200
2400
3600
Time, s
A340
A427
A412